PFC/RR-94-11

# DESIGN OF AN ELECTRONIC CHARGED PARTICLE SPECTROMETER TO MEASURE $\langle \rho R \rangle$, YIELD, AND IMPLOSION SYMMETRY ON THE OMEGA UPGRADE

**D. G. Hicks, C. K. Li, R. D. Petrasso,**

**K. W. Wenzel, J. P. Knauer†**

November 1994

Plasma Fusion Center

Massachusetts Institute of Technology

Cambridge, MA 02139

† Laboratory for Laser Energetics

University of Rochester

Rochester, NY 14623

This work was supported in part by U. of Rochester Contract No. 410025-G, U.S. DOE Contract No. DE-FG02-91ER54109, and LLNL Contract No. B116798.

# Abstract

The preliminary design for a state-of-the-art diagnostic that will measure a broad energy spectrum of charged particles generated in the OMEGA Upgrade facility is investigated. Using a set of photodiodes ($\sim$ 10) and a 0.8 Tesla permanent magnet, the diagnostic will uniquely determine particle energies and identities from 0.2 MeV up to the maximum charged particle energies (10.6 MeV tritons, 12.5 MeV deuterons and 17.4 MeV protons). With its high density picture elements, each photodiode has $10^6$ single-hit detectors, giving the spectrometer a dynamic range of 1 - $10^5$ particles/shot. For example, in the case of a DT yield of $10^9$ neutrons, about 100 knock-on charged particles will be detected when the spectrometer aperture is 60 cm from the implosion. Furthermore, the measurement of knock-on D and T spectra will allow $\rho R$'s up to 0.15 g/cm$^2$ to be measured (for a 1 keV plasma), or 0.3 g/cm$^2$ if hydrogen doping is used. In addition, the yield and slowing down of secondary protons may be used to determine $\rho R$ up to 0.3 g/cm$^2$.

Significantly, this diagnostic will also directly measure the DD fusion yield and energy degradation of nascent 3 MeV protons. By using two such compact spectrometers to measure the yield and spectra on widely separated ports around the OMEGA Upgrade target chamber, the implosion and burn symmetry can be determined. Furthermore, the ion temperature, and, in principle, even the electron temperature can be measured. The diagnostic and its development will be fully tested at several critical steps, utilizing 0.2 - 16 MeV protons (and several other charged particles and neutrons) from our absolutely calibrated Cockcroft-Walton facility.

# 1 Introduction

In order to ignite an inertial confinement fusion target using realistic amounts of driver energy, the fuel must be compressed to 500 – 1000 times the liquid fuel density. At these densities, the fuel density-radius product $\rho R$ is equal to or greater than the range of fusion product $\alpha$ particles (0.2 - 0.3 g/cm$^2$) and self-heating of the fuel occurs. Thus the fuel $\rho R$ is a crucial parameter in measuring the progress of inertial confinement fusion towards ignition and burn.

Techniques for measuring $\rho R$ use fusion products rather than x-rays. While x-ray diagnostics can be invaluable in the analysis of implosion dynamics leading towards maximum compression, measurement of core conditions at maximum compression requires the use of fusion products since at such high densities, the x-ray mean free path is usually less than the target radius. Energetic fusion particles typically have longer mean free paths and can emerge from the compressed plasma carrying the information from the core during the period of fusion reactions. There are a number of different techniques for determining $\rho R$. The knock-on [1, 2, 3, 4] and secondary reaction methods [5, 6, 7] utilize charged particles and are the focus of the spectrometer discussed herein. Beyond $\rho R \sim 0.4$ g/cm$^2$, however, charged particles are thermalized or severely slowed down within the high density fuel. At higher $\rho R$'s, neutron diagnostics such as neutron activation [8], elastically scattered DT neutrons, and extra high energy neutrons (up to $\sim$ 31 MeV) generated by tertiary reactions of knock-on deuterons and tritons [7] are the preferred methods.

The knock-on and secondary reaction techniques demand that there be a diagnostic which can, at the very least, measure the number of charged fusion products above a particular energy, although a mere yield will leave the experimenter in serious doubt as to the precise origin of the charged particles. Therefore, with the numerous different types of charged particles, and the copious, obscuring background of neutrons and x-rays generated by inertially confined plasmas, it becomes highly desirable for a successful $\rho R$ diagnostic to be able to uniquely determine, almost instantaneously, the identity and energy of more than one hundred (preferably a thousand) charged particles. To date, only CR-39 track etch detectors [3] and nuclear emulsion detectors [4] have been used. These involve laborious off-line analysis techniques. In addition, their energy resolution is limited (usually no better than 1 - 2 MeV), and they have to operate within a very restricted energy window (3 - 5 MeV) in order to effectively discriminate against the background. This report investigates an electronic charged particle spectrometer which will enable immediate analysis of the identity and energy of anywhere from 1 – $10^5$ protons, deuterons and tritons from 0.2 MeV up to their maximum energies (17.4 MeV for protons, 12.5 MeV for deuterons, and 10.6 MeV for tritons).

The report first outlines the theory behind the knock-on and secondary reaction diagnostic techniques, emphasizing their assumptions and how they lead to upper limits on the measurable $\rho R$. This is followed by a brief outline of how the fusion yield, implosion symmetry, and ion temperature may be determined using the charged particle spectrum. Considerations for the use of charge-transfer arrays in charged particle detection will then be discussed, leading to the proposed design which incorporates ten or more photodiode arrays and a 0.8 Tesla permanent magnet.

# 2 The knock-on and secondary reaction methods for $\langle \rho R \rangle$ measurements

Previous experiments to measure $\rho R$ using charged particles have either relied upon the knock-on or the secondary reaction method. These methods require the detector to count the number of charged particles escaping from the target that are generated by a particular process (elastic scattering by neutrons or D-$^3$He secondary reactions). Spectral resolution is necessary in order to unambiguously identify the detected charged particles with the processes of interest.

This section describes the theory and underlying assumptions behind these two methods. Particular attention will be made to the improvements that can be made if a well resolved charged particle spectrum can be obtained.

## 2.1 The knock-on method

The principle of this method is to measure the number of deuterons and tritons from the fuel which have been elastically scattered by the 14.1 MeV neutrons generated in the primary fusion reaction [1, 2, 3, 4]. In order to be certain whether the emitted ions are actually elastically scattered, the energy spectrum of the particles must be analyzed and compared to the predicted spectrum. While the measurement of an energy spectrum is not absolutely necessary, a well resolved spectrum greatly improves the quality of the measurements and allows a higher $\rho R$ to be measured.

Assuming that all neutrons are generated at the center of the target (centrally ignited model), the number of unscattered neutrons at a radius $r$ is given by

$$Y(r) = Y_0 \exp\left(-\int_0^r (\sigma_d n_d(r') + \sigma_t n_t(r'))dr'\right). \tag{1}$$

Note that at these high energies, the cross section for elastic scattering dominates over that for other interactions and thus the depletion of this neutron 'stream' may be considered as solely due to elastic scattering. Since the probability for neutron scattering within fuel of $\rho R \sim 0.1$ g/cm$^2$ is very small, it is a good approximation to take Y(r) = $Y_0$. Now, the number of elastically scattered particles generated along a radius dr about r is given by

$$dQ = Y_0[\sigma_d n_d(r) + \sigma_t n_t(r)]dr \tag{2}$$

Integrating Eq.(2) over radius from 0 to R, the maximum radius of the fuel, the total number of knock-ons generated is given by

$$Q = Y_0 \int_0^R [\sigma_d n_d(r) + \sigma_t n_t(r)]dr \tag{3}$$

Letting $\gamma = \frac{n_d}{n_t}$ (which is not a function of r), and taking $\sigma_d$ and $\sigma_t$ as constants (a good assumption since multiple scattering does not occur for $\rho R$'s of interest) gives

$$Q = Y_0(\gamma\sigma_d + \sigma_t) \int_0^R n_t(r)dr \tag{4}$$

Defining

$$\langle \rho R \rangle = \int_0^R (m_d n_d(r) + m_t n_t(r)) dr = (2\gamma + 3) m_p \int_0^R n_t(r) dr, \tag{5}$$

gives[1]

$$Q = \frac{Y_o(\gamma \sigma_d + \sigma_t)}{(2\gamma + 3) m_p} \langle \rho R \rangle. \tag{6}$$

Now the number of knock-ons generated is different from the number that actually emerge from the target, since the lower energy knock-ons range-out before they can escape. Thus there is a minimum energy threshold for the detected knock-ons according to the fuel and pusher $\rho R$. The adjustment to Q can be made by replacing the total cross sections for elastic scattering by effective cross sections to generate ion energies above the threshold for escape. In actual fact, the effective cross sections, $\sigma_d^{eff}$ and $\sigma_t^{eff}$, will be determined by the detector threshold. The energy and angular differential cross sections are given in Figs. 1 and 2[2] and the effective cross sections, calculated by integrating the differential cross sections from the peak knock-on energy down to the threshold for detection, are given in Fig. 3. (Note that the threshold for detection will always be higher than the threshold for escape. In the design that follows, the lower detection threshold can be as low as 0.2 MeV.) The number of knock-ons detected is further reduced by the detector fractional solid angle. Thus,

$$\langle \rho R \rangle = \frac{(2\gamma + 3) m_p}{Y_0(\gamma \sigma_d^{eff} + \sigma_t^{eff})} Q_{det} \left( \frac{4\pi}{\Omega} \right) \tag{7}$$

where $Q_{det}$ is the number of knock-ons actually detected, ie. those knock-ons within the energy window for detection and in the detector solid angle. Thus $\rho R$ is directly proportional to the number of detected knock-ons and may be determined provided that the DT neutron yield $Y_0$ is simultaneously measured.

The assumptions leading to Eq.(7) are as follows:

i A spherically symmetric target. Previous $\rho R$ experiments using two CR-39 detectors in different positions around the vacuum chamber appear to make this assumption reasonable. By making this diagnostic compact enough to be moved between different ports, we can verify this.

ii A centrally ignited target. A uniform burn model alters Eq. 6 by a factor of order one. There are clearly many more complicated burn models than these two and the importance of this assumption will depend on the accuracy of results.

---

[1] If the fuel is hydrogen doped, Eq.(6) becomes $Q = \frac{Y_o(\beta \sigma_p + \gamma \sigma_d + \sigma_t)}{(\beta + 2\gamma + 3) m_p} \langle \rho R \rangle$ where $\beta = \frac{n_p}{n_t}$.

[2] The conversion from an angular differential to an energy differential is as follows: If a neutron of energy $E_n$ and mass m elastically scatters off a stationary ion of mass M, conservation of momentum and energy dictates that $1 - (E/E_n) = (1 + \alpha)/2 + \cos\theta(1 - \alpha)/2$,where E is the scattered ion energy, $\alpha$=((M/m)-1)/((M/m)+1) and $\theta$ is the scattering angle of the neutron in the center of mass frame. By defining $\mu = \cos\theta$, the differential energy cross section can be written as $d\sigma/dE = (d\sigma/d\mu)(d\mu/dE) = -(2/((1-\alpha)E_n))(d\sigma/d\mu)$.

Now since the differential cross section is independent of the angle $\phi$ which is azimuthal to the incident neutron direction, $d\sigma/d\mu = \int (d\sigma/d\Omega) d\phi = 2\pi (d\sigma/d\Omega)$where $d\sigma/d\Omega$ is the quantity tabulated in Fig. 2. Thus, the energy differential cross section is given by: $d\sigma/dE = -4\pi/((1 - \alpha)E_n)(d\sigma/d\Omega)$

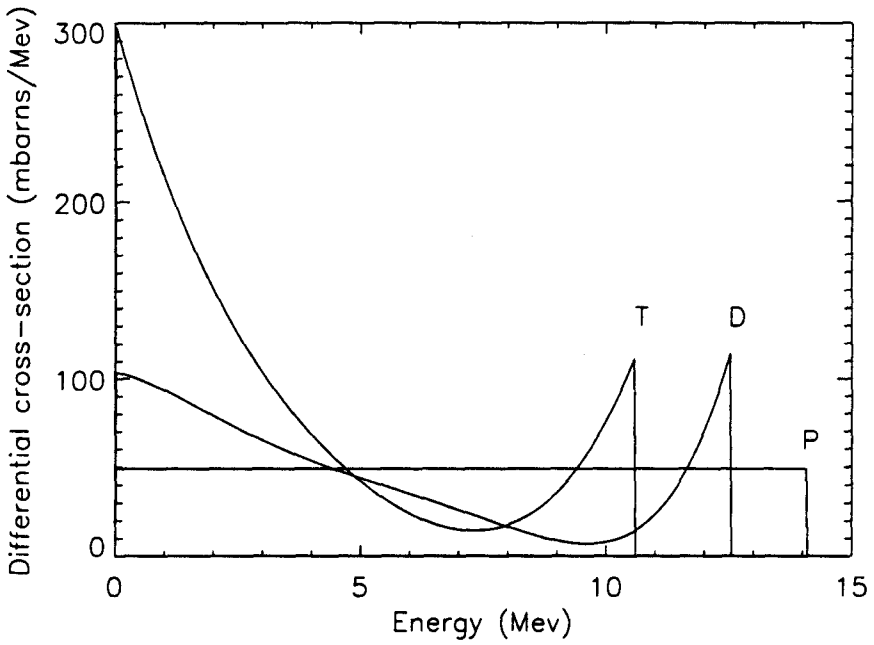


Figure 1: Energy differential scattering cross-sections $\left(\frac{d\sigma}{dE}\right)$ for knock-on protons, deuterons and tritons elastically scattered by 14.1 MeV neutrons. The curves were generated from fits to the neutron angular differential cross section data given in Fig. 2. The high energy cutoff and the lower energy droop in D and T cross sections may be used as reference points to determine the shift in energy of the spectrum in high $\rho R$ experiments. This will allow the calculation of $\sigma^{eff}$ from the knock-on formula.

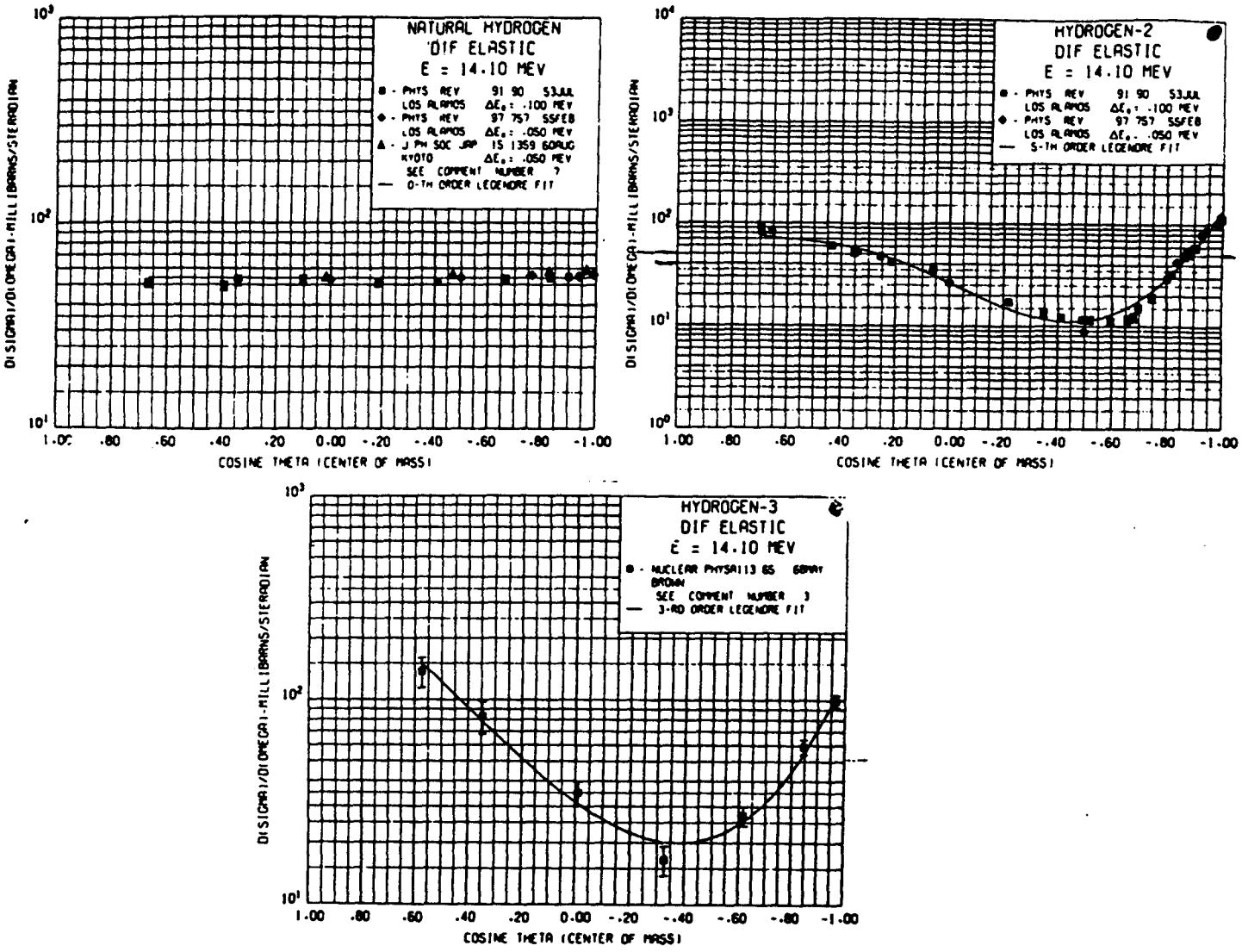


Figure 2: Differential angular neutron elastic scattering cross-sections $\frac{d\sigma}{d\Omega}$ for 14.1 MeV neutron scattering off protons, deuterons and tritons as taken from [9]. Cosine theta represents the scattering angle of the neutron and is directly proportional to the energy of the scattered ion. Note that below $\cos\theta \simeq 0.6$ (E$\simeq$ 2 MeV), no experimental data exists so the energy differential cross section data in Fig. 1 is represented by an extrapolation in this region.

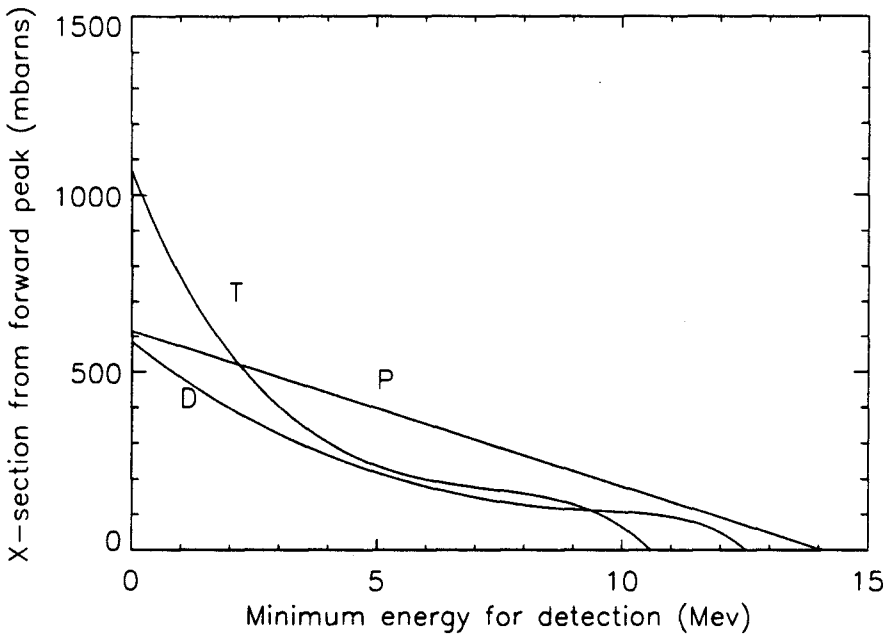


Figure 3: The effective scattering cross-section for knock-ons as given by $\sigma^{eff}(E) = \int_E^{E^{max}} \frac{d\sigma}{dE'} dE'$. This is used in the calculation of the knock-on signal (Eq. 7) if only knock-ons above an energy E are viewed by the detector. Note that the total elastic cross section for 14.1 MeV elastic scattering is 0.6 barns for protons, 0.63 barns for deuterons and 0.92 barns for tritons.

iii The probability for neutron scattering is very small, implying a large mean free neutron path to target radius ratio and thus a small $\rho R$. For $\rho R$ leading to ignition, burn and even far beyond, this assumption introduces negligible error.

iv All knock-ons within the detector solid angle and above the detector threshold energy, escape from the fuel and pusher and are recorded by the detector.

At high $\rho R$'s, when the charged particle spectrum is downshifted and distorted, the knock-on relation in Eq. 7 holds provided that the effective cross section, $\sigma_{eff}$, can be determined correctly. A critical function of the proposed high resolution charged particle spectrometer, which can measure energies down to 0.2 MeV, is to observe this downshift in spectra. By using the high energy cutoff and the lower energy droop in the knock-on D and T spectra (shown in Fig. 1) as reference points to define $\sigma_{eff}$, Eq. 7 may be used even in severely downshifted spectra, provided that this high energy 'ramp' may still be identified.

The energy loss for the maximum energy knock-ons as a function of $\rho R$ is calculated in Ref. [4] by a monte carlo simulation. The results of these calculations are shown in Fig. 4. It is possible that by observing the shift in spectra and determining $\rho R$ using the method above, the accuracy of this, or other, stopping models may be verified. In addition, with a suitable stopping model, $\rho R$ may be directly measured from the energy degradation of the charged particles. Furthermore, it is, in principle, possible to determine the electron temperature from this shift in spectrum.

By successful measurement of energy spectra of D and T, the knock-on method may be extended up to a limit of about $\rho R \sim 0.15$ g/cm$^2$, at which point even the high energy deuterons would not escape. A new method for pushing the knock-on limit up to $\rho R \simeq 0.3$ g/cm$^2$ or more was proposed in Ref. [4]. In this experiment, the target was filled with a 1:1:1 mixture of H:D:T and it was the knock-on protons that were measured. As can be seen in Fig. 4, protons are able to emerge from targets with higher $\rho R$'s. This diagram shows that using proton knock-ons would increase the knock-on $\rho R$ limit to 0.3 g/cm$^2$ for plasmas above 1 keV.

In all these calculations, it is important to recognize that the pusher $\rho \Delta R$ has not been considered. Depending on the types of pushers used this could lower the $\rho R$ limit.

Since the cross section for proton scattering is about that for deuterons ($\simeq 0.6$ barns), unless neutron yields are much greater than $10^{11}$ per shot, approximately equal quantities of protons, and D and T ions would need to be present to provide a suitable signal (signal calculations to follow).

## 2.2 The secondary reaction method

The basis for the secondary reaction method is described in Ref.[5] and experimental results are given in Refs.[6] and [7]. The method essentially involves counting the number of protons generated by the D-$^3$He secondary reaction, and comparing it to the number of primary DD reactions. Once again, measurement of the spectrum of particles will greatly improve the confidence and accuracy of this method as well as raise its upper $\rho R$ limit.

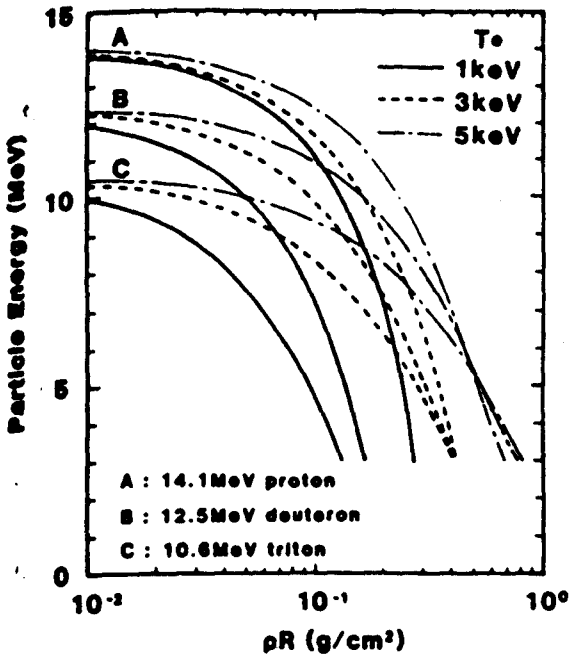


Figure 4: Monte Carlo simulation for the energy slowing down of knock-on particles in a D, T, H mixture plasma at different electron temperatures [4]. In principle, the energy degradation of charged particles may be used to determine $\rho R$ or $T_e$. Note that protons usually have a much higher $\rho R$ limit for range-out.

The reaction utilized is the following:

$$^3He^*(< 0.82\text{MeV}) + D \rightarrow \alpha + p(12.5 - 17.4\text{MeV})^3 \tag{8}$$

where the 0.82 MeV $^3$He is derived from a branch of the primary DD reaction. Another important secondary reaction is derived from the high energy triton in the other main branch of the DD reaction:

$$T^*(< 1.01\text{MeV}) + D \rightarrow \alpha + n(11.8 - 17.1\text{MeV}) \tag{9}$$

though this produces a secondary neutron and thus is not the main interest of this charged particle detector.

The ratio of the secondary to primary reaction rates, given by the ratio of high energy protons to 2.5 MeV neutrons from DD, is directly related to the fuel $\rho R$ as follows.

Assuming that all primary fusion reactions occur in the center of the target, the number of $^3$He particles streaming outward at a radius $r$ is given by:

$$Y(r) = R_{DDn} \exp\left(-\int_0^r \sigma_{DHe}(r')n_d(r')dr'\right), \tag{10}$$

where $\sigma_{DHe}$ is the cross section for the secondary fusion reaction and $R_{DDn}$ is the number of neutron ($^3He$) forming DD reactions. This assumes that fusion is the dominant process for removing $^3$He ions[4]. Now, since the branching ratio for the D(D,n)$^3$He and D(D,p)T reactions is almost 50 %, $R_{DDp} \simeq R_{DDn}$, where $R_{DDp}$ is the number of proton producing DD reactions. This is critical since this charged particle detector will be able to directly measure $R_{DDp}$ and will not need to depend on neutron measurements of $R_{DDn}$. The following discussion will thus use $R_{DDp}$. Thus, the number of D$^3$He reactions which occur in a target of radius R is given by:

$$R_{DHe} = R_{DDp}(1 - \exp(-\langle\sigma_{DHe}n_dR\rangle)) \tag{11}$$

where

$$\langle\sigma_{DHe}n_dR\rangle = \int_0^R \sigma_{DHe}(r)n_d(r)dr \tag{12}$$

Assuming that the $^3$He ion suffers little degradation in its initial energy such that its fusion cross section remains constant throughout the fuel,

$$\frac{R_{DHe}}{R_{DDp}} = \frac{\gamma\sigma_{DHe}}{(2\gamma+3)m_p}\langle\rho R\rangle \tag{13}$$

where $\gamma = \frac{n_d}{n_t}$ and $\sigma_{DHe} \sim 0.78$ barns (the fusion cross section for a 0.82 MeV $^3$He ion incident on a stationary D ion) and $\langle\rho R\rangle$ is defined as in Eq.5. Thus it can be seen that for low $\langle\rho R\rangle$ (below about 0.01 g/cm$^2$), the fraction of secondary to primary reactions is directly proportional to $\langle\rho R\rangle$.

Once again, the assumptions and their validity will be summarized:

[3]The spread in secondary fusion product energies comes from the non-zero initial energy of the primary fusion product.

[4]Note that elastic scattering has a far greater interaction cross section, though it doesn't directly remove $^3$He ions. However, at high $\rho R$'s, elastic scattering will significantly slow down the $^3$He ions within the fuel and thus make the fusion cross section strongly dependent on radius - a process which limits the usefulness of this method at high $\rho R$'s as explained later.

i A spherically symmetric target. This can be verified with measurements from two different angular positions.

ii A centrally ignited target. The uniform burn model changes Eq. 13 by a factor of order one. Results may lead to some information about the spatial burn profile.

iii The probability for fusion of the $^3He$ during its passage through the target is small, implying a large mean free path to target radius ratio and thus a small $\rho R$.

iv The fusion cross-section is calculated for a monoenergetic $^3$He beam at 0.82 MeV, assuming no slowing down of the $^3$He ions. This is effectively an equivalent assumption to the one directly above.

v All secondary protons within the detector solid angle are emitted from the fuel and recorded by the detector.

In the case of neutron scattered D and T ions, it was the stopping of the knock-ons, which provided the ultimate upper $\rho R$ limit to the diagnostic. In this case, it is the 0.82 MeV $^3$He primary products which provide the limit, since they slow down more readily than the high energy secondary protons. Thus for higher $\rho R$, the third and fourth assumptions break down. Above this $\rho R$, the relationship of secondary to primary reaction yields to fuel $\rho R$ has been calculated numerically in Ref. [7] by taking into account slowing down of primary fusion products and the consequent change in the D$^3He$ fusion cross section. The results are shown in Fig. 5a. It can be seen that for $\rho R < 0.01$ g/cm$^2$, the yield ratio is proportional to $\rho R$ as derived above but with increasing thermalization in denser targets, the yield ratio saturates and becomes a function of temperature. Thus the maximum $\rho R$ using only secondary protons is about 0.02 g/cm$^2$ for a 3 keV plasma. With an independent calculation of the temperature, $\rho R$ could be measured well into the thermalization region. One way of doing this is to simultaneously measure the secondary neutron reaction yield from primary tritons produced in the other DD branch reacting with background deuterons. (Of course, now a pure deuterium target must be used.) The relationship of this secondary neutron yield to fuel $\rho R$ is shown in Fig. 5b. It can be seen that due to the greater range of primary tritons in the fuel, the secondary neutron reaction yield maintains its dependence on $\rho R$ to a higher density limit before saturation. By calculating the temperature from the $D^3$He curves, assuming thermalization, $\rho R$ can be found from the DT yield curves. For a 3 keV plasma, this would allow a $\rho R$ up to 0.1 g/cm$^2$ or more to be measured. Beyond this point, the uncertainties in the two yield measurements would limit the method.

Without appropriate neutron diagnostics, the usefulness of this method appears to be limited to $\rho R \simeq 0.01$ g/cm$^2$. However, this limit could be extended much further if the slowing down of the secondary protons (and not merely the ratio of the proton to neutron yield) could be measured. Once again, it is absolutely necessary to have a spectrometer in order to do this. This method would involve examining the shift in the spectrum of 12.5 - 17.4 MeV protons and comparing it to a theoretical stopping model (or even to results from the knock-on method). This would raise the $\rho R$ limit since such high energy protons will not range-out until above $\rho R = 0.3$ g/cm$^2$.

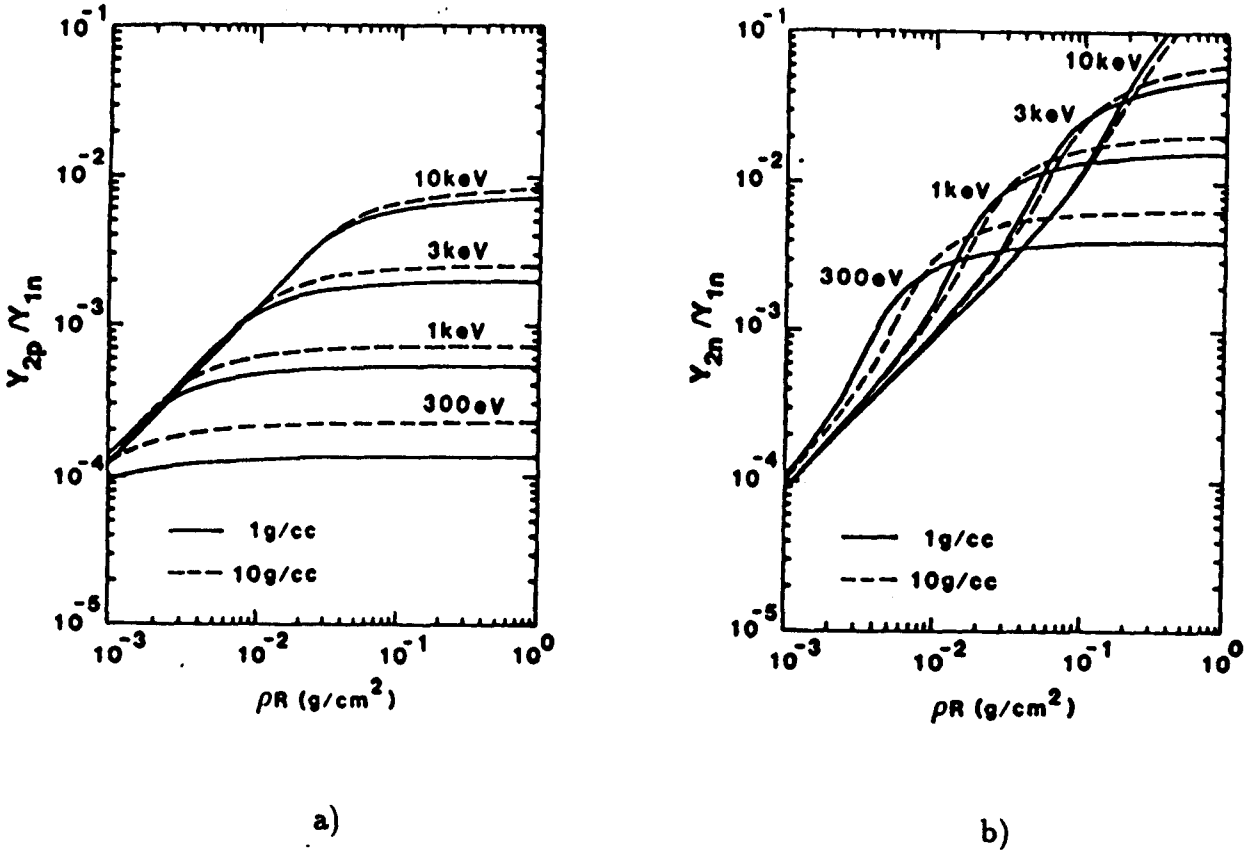


Figure 5: a) Calculated yield ratio of secondary protons to primary neutrons (or primary protons since the D(D,n)$^3$He and D(D,n)T branching ratio is about 50 %) as a function of fuel $\langle \rho R \rangle$ for DD fuel (from [7]). The model assumes a uniform density and temperature fuel with primary reactions taking place uniformly in the entire fuel region. Notice that $^3$He ions are completely stopped within the fuel above $\rho R \simeq 0.03$ g/cm$^2$. Beyond this point (and even before this), $\rho R$ may be measured by determining the shift in the secondary proton spectrum, which at low $\rho R$, has a peak of 17.4 MeV. At these high $\rho R$'s, the yield of secondary protons may be used to directly determine the total fusion yield. b) Calculated yield ratio of secondary-to-primary neutrons as a function of fuel $\langle \rho R \rangle$ [7]. Tritons have a longer range than $^3$He ions and this ratio maintains its $\rho R$ dependence to higher $\rho R$'s. The two secondary-to-primary reaction ratios may be compared to determine $\rho R$ and $T_e$ at high $\rho R$'s.

| $T_e$ (keV) | $\rho R$ (g/cm$^2$) for range-out |
|---|---|
| 1.0 | $\sim 0.03$ |
| 3.0 | $\sim 0.1$ |
| 5.0 | $\sim 0.2$ |

Table 1: $\rho R$'s for the range-out of 3 MeV protons from our preliminary calculations

# 3 The charged particle spectrum: Measurements of fusion yield, implosion symmetry and $T_i$

In addition to measurements of $\rho R$ and $T_e$, measurement of a wide, highly resolved charged particle spectrum gives the fusion yield and $T_i$ as well. Fusion yield and spectral measurements at different positions around the vacuum chamber can be used to address the issue of implosion symmetry.

## 3.1 Fusion yield measurements using charged particles

With a well resolved charged particle spectrum in the 0.2 - 3 MeV region, the fusion yield can be measured from the yield of 3 MeV DD protons. In the past, yields have largely been measured by neutron diagnostics; however, with a charged particle yield diagnostic, a greater dynamic range may be attained since at high yields, the charged particles may be collimated to avoid detector saturation. In addition, by using the proposed photodiode arrays, there will be $10^6$ or more single-hit detectors available.

Most importantly, the proposed detector will, in principle, be able to measure protons down to 0.2 MeV. Thus, even with the energy degradation of proton energy at high $\rho R$'s, the shifted 3 MeV proton spectrum can still be resolved. The $\rho R$'s for 3 MeV protons over a range of temperatures and densities are depicted in Fig. 6 as calculated from C.K.Li's $\rho R$ code. Some results are summarized in Table 1.

For higher $\rho R$'s, the fuel may be doped with $^3$He to produce 14.7 MeV protons which do not range out until $\rho R \simeq 0.3$ g/cm$^2$.

An important role of these yield measurements is to compare the yield results from this charged particle detector with those from neutron measurements. Good agreement will ensure confidence in both methods.

## 3.2 Implosion symmetry

In principle, a fusion yield diagnostic will also measure the implosion symmetry if the diagnostic can be placed at different positions around the vacuum chamber. With the magnet and photodiode design proposed, the diagnostic could readily fit into a TIM and will thus be portable. Furthermore, by measuring $\rho R$ concurrently with fusion yield, more detailed information about the nature of the implosion asymmetry can be obtained.

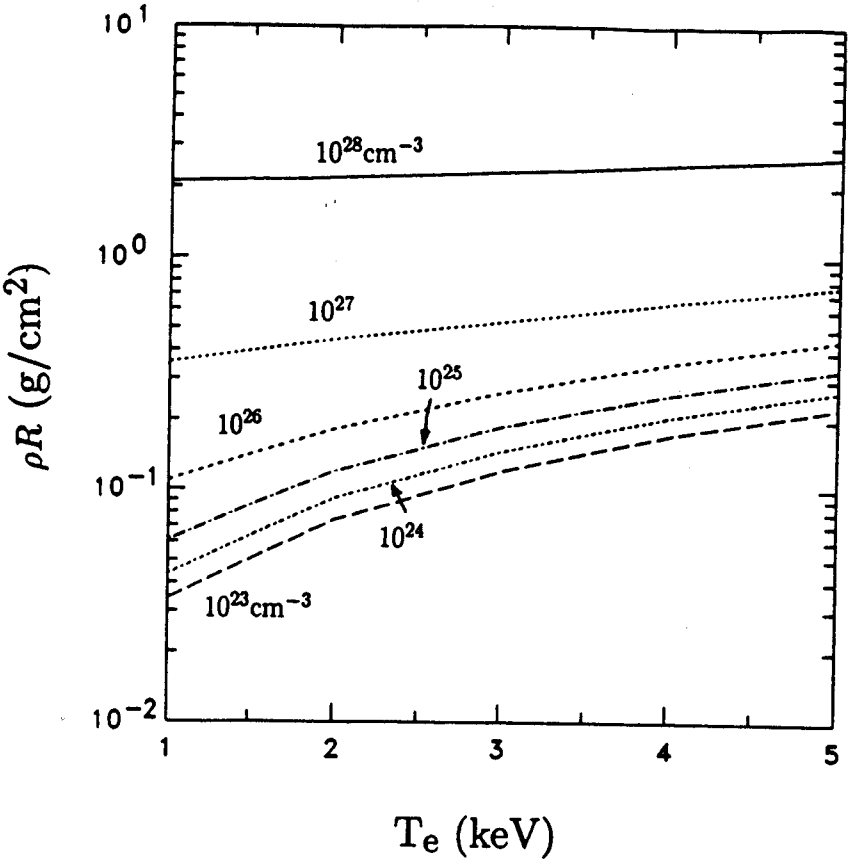


Figure 6: $\rho R$ curves for 3.0 MeV protons interacting with a deuterium plasma at various temperatures and densities. Quantum degeneracy effects are important for $n_e > 10^{26}$ cm$^{-3}$

## 3.3 Ion temperature measurements using charged particles

With a spectrum of high resolution, it may be possible to measure the ion temperature from the line width of the 3 MeV DD proton. The DD reaction is given by:

$$D + D \rightarrow T + p \quad (Q = 4.0MeV). \tag{14}$$

For a Maxwellian plasma at temperature T, the spectrum of DD protons is given by a Gaussian [10]:

$$P(E_p) \sim \exp\left[-\left(2m_d(E_p - < E_p >)^2\right) \Big/ \left(\frac{4m_t m_p}{m_t + m_p} QT\right)\right] \tag{15}$$

where $m_p$, $m_d$ and $m_t$ are the respective masses of the proton, deuteron and triton, $E_p$ is the energy of the proton and $\langle E_p \rangle$ is the average energy of the proton ($\sim$ 3 MeV).

Therefore, the full width half maximum of this spectrum, which is centered around $\langle E_p \rangle$, is given by

$$\Delta E_p = 2\sqrt{\ln 2 E_p T} \tag{16}$$

where $E_p = \frac{m_t}{m_t + m_p} Q$ = 3 MeV. Thus at 1 keV, $\Delta E_p \simeq$ 92 keV. Preliminary calculations (shown in section 8.2) indicate that by using a high resolution CCD array (such as the RA 2000J manufactured by EG&G Reticon), this energy difference may be spread over 15 pixel elements on either side of the 3 MeV peak.

# 4 Results from previous experiments and the limitations of track detectors

## 4.1 Previous experimental results

The detailed method of utilizing filters and spatial coincidence to detect knock-ons in CR-39 track detectors is described in Ref. [3]. In this experiment, only deuterons with energies from 4.6 - 6.9 MeV and tritons from 5.4 - 10.3 MeV could be viewed, resulting in 91 tracks[5]. The error in $\rho R$ from this was estimated to be about 25 - 30% while the signal-to-noise ratio was estimated at 20:1 [2].

Proton knock-on results using nuclear emulsions are given in Ref. [4]. In this experiment, with neutron yields of $10^{10}$ - $10^{11}$, 31 knock-on deuterons were produced in the 9.0 - 12.5 MeV window and 118 knock-on protons in the 10.0 - 14.1 MeV window. Due to the lower bound on the energy window dictated by the detector, even using knock-on protons raised the maximum $\rho R$ to only 0.15 g/cm$^2$.

The results of experiments using the secondary reaction method are given in [6] and [7]. Typically, 100 - 1000 particles were measured at DD neutron yields of $10^9$, with an uncertainty in $\rho R$ of about 20%.

## 4.2 Limitations of track detectors

The main limitations to the accuracy of $\rho R$ measurements so far have been imposed by the detector, not the physical limits described above which are likely to occur at higher $\rho R$. The following is a summary of the main problems:

i Time-consuming, manual data processing involving measuring track diameters by microscope.

ii Low energy resolution ($\sim$ 1 MeV) due to uncertainty in track diameter.

iii Difficulty in identifying particles with the same velocity but different masses. Eliminating the proton background from the knock-ons required precise thicknesses of CR-39 and severely restricted the energy window.

iv Particles incident at greater than a critical angle are not recorded. This can be a problem with the use of filters which scatter the incident particles.

Ref. [4] claims that nuclear emulsions do not suffer from many of these problems, but the most critical shortcoming, the laborious manual data processing, is still present.

[5]The restrictive energy windows are the result of the ambiguity in discriminating the proton background from the knock-ons and the subsequent need to cut precise thicknesses of CR-39 layers to measure spatially coincident tracks.

# 5 Requirements for a charged particle spectrometer

## 5.1 Particle identification and energy resolution at high flux

In order to obtain a reasonable energy spectrum of the knock-on or secondary reaction ions, a detector must determine the energy (and preferably mass) of more than $10^3$ particles[6]. Since the target compression and burn times are on the order of 1 ns, a real time analyzer, such as a time-of-flight detector, would need time resolution in the sub-nanosecond range and even then might not be able to capture all the particles necessary for good spectral resolution. It is more reasonable to use a detector which captures and stores the particle information for readout in the ample time between shots. The common silicon surface barrier diode is the most widely used charged particle spectrometer; however, due to the high particle fluxes involved here, there will inevitably be pulse pile up if an SBD were to be used. Even the use of a magnetic spectrometer to disperse the particle flux onto a large array of SBD's would not be sufficient since there would almost certainly be enough particles (ie. two or more) within the particular SBD windows to cause pulse pile-up.

## 5.2 Background noise discrimination

A summary of background noise sources is given in Fig. 7. The greatest potential sources of noise will be pusher protons, neutrons, visible light (semiconductor arrays are particularly sensitive to this), x-rays and ion blow-off. A bending magnet will remove the detector from the line-of-sight of x-rays and bend low energy ions (keV) and electrons far enough away from the detector. Visible light will be attenuated by many orders of magnitude using a 1500 Å aluminum window on free standing mesh. First estimates predict that within the thin sensitive region of the semiconductor array, neutron background is unlikely to be a problem until very high neutron yields are achieved. If need be, shielding could be employed.

The largest source of proton background is likely to come from knock-ons from the CH pusher. Tests should be performed using neon-filled targets to gain an estimate of the signal from non-fuel proton knock-ons. A quick estimate for the pusher knock-on contribution can be gained by considering that typical CH shells have a density of 1.02 g/cm$^3$ and a thickness of $\approx 20$ $\mu$m, leading to a $\rho\Delta R$ of 2 mg/cm$^3$. By analogy with Eq. (6), the number of pusher knock-on protons is given by $Q_{pusher} = Y_0 \frac{\sigma_p}{m_c+m_p}\langle\rho\Delta R\rangle$, while the number of fuel knock-on protons from a fuel with equal quantities of D, T and H is given by $Q_{fuel} = Y_0 \frac{\sigma_p}{m_t+m_d+m_p}\langle\rho R\rangle$. Thus, $\frac{Q_{pusher}}{Q_{fuel}} = \frac{6}{14}\frac{\rho\Delta R}{\rho R} = 9$ % at $\rho R = 10$ mg/cm$^2$. For DD yield measurements, it is useful to note that the number of DD fusion protons is of a similar order to the number of fuel knock-ons in DT targets. Thus the ratio of signal to background protons would follow the same dependence as that calculated above.

It will need to be investigated whether or not there are other sources of low energy protons.

[6]With the large variations between shots in an ICF experiment, it is useful to have a detector which can not only measure $> 10^3$ particles (or even $10^5$ for high yields) but also measure 1 – 100 particles to diagnose a poor implosion.

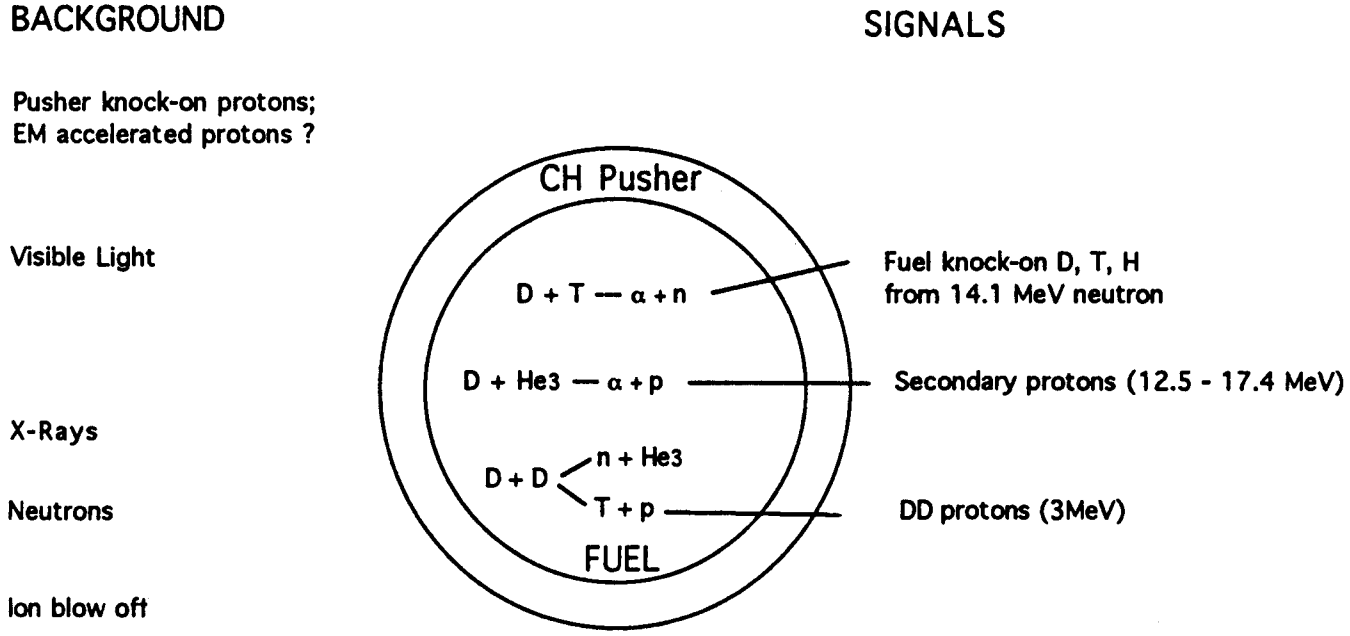


Figure 7: Sources of signal and background for a detector in an ICF environment. With a bending magnet to remove the detector from the target line-of-sight (and disperse low energy ions), the main sources of background will be MeV protons and neutrons. Reflected laser light will be eliminated by a 1500 Å aluminum window on free standing mesh.

# 6 General considerations for semiconductor arrays as high flux, charged particle spectrometers

The problem of individual particle detection in a dense flux environment is common to particle physics and numerous possible detectors have been used for this purpose. These include track etch detectors, nuclear emulsion, photographic film, gas-filled wire chambers and various types of semiconductor arrays (CCD's and photodiodes). Semiconductor arrays are the most attractive because of their electronic readout; however the technology for these arrays is strongly geared towards imaging of photons rather than spectroscopy of particles. The major design challenge for this diagnostic is to determine whether or not a semiconductor array is suitable for high flux, charged particle spectroscopy.

A number of CCD and photodiode array manufacturers were investigated, including Lincoln Labs (MIT), EEV, SITE (Tektronix), Princeton Instruments and EG&G Reticon. It was found that EG&G had a large variety of commercially available products, and thus much of the following general product data is taken from their catalog [11].

## 6.1 Number of pixels

In order for an array to resolve the energy of individual particles, each pixel must typically receive no more than one incident particle. For example, if $10^3$ - $10^4$ particles are incident on an array 2 cm on a side, each element must be smaller than 200 $\mu m$. Since the particles or their deposited charge might cross over into adjacent elements (blooming), and since there will certainly be some background particles, more elements would better resolve the passage of an individual particle. Thus, an array must have $10^5$ elements or more. Typical photodiodes have about $5\times10^4$ to $5\times10^5$ elements, while CCD's have from $10^5$ to $10^6$ pixels. Typical arrays are from 1 - 2 cm on a side with 15 - 50 $\mu m$ elements. Thus if a few arrays could be lined up side-by-side, there should not be any problem with the number of elements in either photodiodes or CCD's. Clearly, if fluxes much higher than 1000 particles per shot actually occur, the detector solid angle may be reduced to prevent saturating the arrays.

## 6.2 Thickness of arrays vs. particle ranges

The range of knock-on deuterons and tritons and secondary protons in silicon is shown in Fig. 8. The semiconductor array and substrate is approximately 1500 $\mu$m thick. Thus practically all but the highest energy protons are stopped well within a typical array thickness. Even thinned, back-illuminated CCD's whose sensitive region is only 13 $\mu m$ thick, still have supporting structures of about 1000 $\mu$m in thickness. Therefore it appears impossible to use a stack of CCD's to track the particle's trajectory as is done in high energy physics. Custom built arrays typically cost anywhere from a half to two million dollars. The stacked detector tracking system provides a number of advantages, such as over-determination of particle identities and energies and good background discrimination. We will continue to investigate whether such thin ($\sim$ 50 $\mu$m) CCD's are available.

With such cost and practical considerations, a method of using just a single layer array and a strong magnetic field is proposed in the next section.

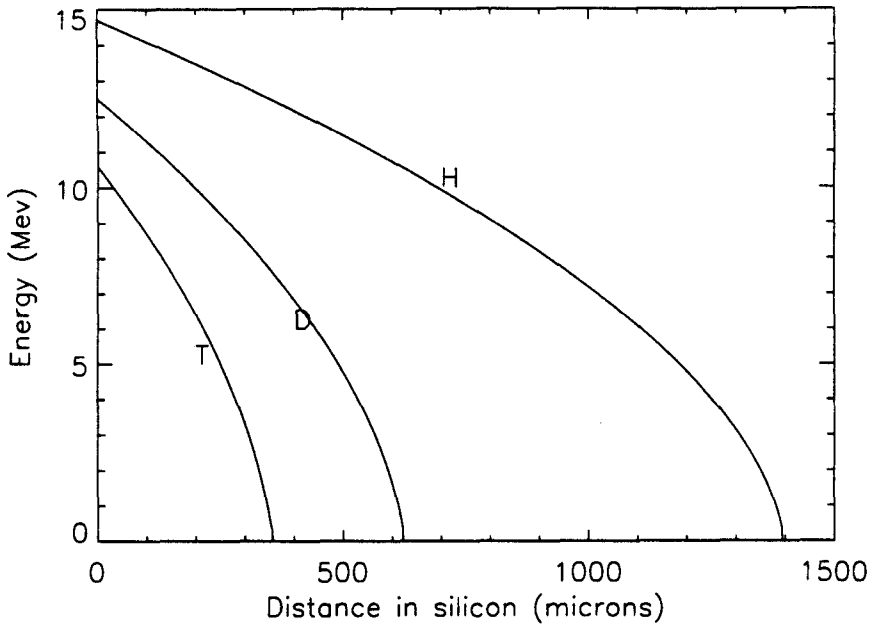


Figure 8: Range in silicon of D and T ions elastically scattered by a 14.1 MeV neutron (maximum energies of 12.5 MeV and 10.6 MeV respectively) along with the range of a 14.7 MeV secondary proton. Ranges are calculated through integration of the Bethe-Bloch formula. The typical thickness of semiconductor arrays and their support structure is over 1500 $\mu$m.

## 6.3 Sensitive depth and saturation capacity of pixel elements

A cross-section through a typical CCD shows the overlying polysilicon electrodes, followed by a depletion layer surrounding the potential well underneath the electrode, beneath which is a diffusion layer and then the supporting substrate. A high-energy charged particle will pass through all of this and yet there is only a sensitive depth, consisting of the depletion layer and some of the diffusion layer (if any), which will produce electron-hole pairs that will be trapped in the potential well and recorded. In order to find the LET (linear energy transfer, or stopping power) of a particle through this structure, it is critical to find the sensitive depth. Typically, the depletion depth is about 10 $\mu m$ or less and, for a first estimate, it can be assumed that the diffusion region is another 10 $\mu m$. Now the LET of a 1 MeV triton is 70 keV/$\mu m$ which, over a distance of 20 $\mu m$, will produce about $4\times10^5$ electrons. The well capacity of CCD's ranges from 1.75 $\times10^5$ to $5\times10^5$, electrons, indicating that most charged particles will be well below saturation capacity. Photodiodes, on the other hand, have a saturation capacity of approximately $50\times10^6$.

It is critical to establish whether charged pairs made in the diffusion region contribute to the signal, and, if they do, what the effective sensitive depth is. Refs. [12] and [13] examine the effects of MeV protons on CCD's. Both conclude that the generated charge is linear with LET for the particular proton energies chosen. It should be of highest priority to experimentally determine this over a wide range of charged particles from the MIT Cockcroft-Walton fusion product source. Should the sensitive depth prove to be indeterminate, or highly variable, it may be necessary to go to thinned CCD's which are typically \$10,000 or more (as compared to \$2000 for unthinned devices)[7]. Our colleagues at Lincoln Labs, MIT, have developed a high quality, thinned, back-biased CCD which will eliminate the problem of charge creation outside the depletion region. We feel confident that such CCD's will eliminate the problem of an indeterminate sensitive depth. It is possible that some of these devices may be purchased or borrowed if the need should arise.

## 6.4 Blooming

Charge pair production in the diffusion layer can also generate blooming. Since the incident particle penetrates all the way through the array, electrons generated deep within the diffusion layer could spread to nearby elements, not just the one directly above. This problem might be alleviated by ensuring that there are many more pixels than incident particles such that charge from adjacent incident particles do not overlap. An effective sensitive depth would need to be carefully evaluated for this effect. The manufacturers claim that blooming is less of a problem in photodiodes whose self-contained diodes enable the charge generated within one element stay within that element; however, it has yet to be determined whether this remains true for charged particle energy deposition. Blooming occurred over 10 or more pixels in Ref. [12] but Ref. [13] claims no blooming occurred for protons and $\alpha$ particles. This issue also needs to be resolved experimentally on our Cockcroft-Walton fusion product

[7]Thinned CCD's have a depleted region of 10 - 20 $\mu$m which is backed up immediately by a plastic, non-charge producing substrate. Thus the sensitive region can be considered as solely due to the depleted region.

facility. Should blooming prove to be a problem, thinned CCD's, such as those from Lincoln Labs (MIT), would need to be considered once again.

### 6.5 Radiation damage

Radiation damage is unlikely to be a problem in this application. There is considerable literature on the effect of radiation on CCD's. Refs. [13] and [14] both claim that radiation damage does not become visible (as an increase in dark current and voltage shift) until irradiation levels of about $10^4$ rad (single particle damage, which occurs with high LET heavy ions, are not observed with protons). This is far above what would be observed over the typical lifetime of an ICF diagnostic.

### Summary

From these brief considerations, the photodiodes would tend to be favored because of their greater well depth and their reduced susceptibility to blooming (which would have to be verified). In the next section, a photodiode array is suggested mainly because its front face has a large sensitive to non-sensitive area ratio.

## 7 Detector concept: A single layer photodiode coupled to a magnetic spectrometer

### 7.1 Measurement of energy and particle identity using a single layer photodiode - partial energy and mass resolution

Since the sensitive depth for a photodiode is only about 20 $\mu m$, an array will only sample the initial LET (linear energy transfer) of an incident particle. The relation between LET and particle energy for stopping of a charged particle in solids is given by the Bethe-Bloch formula, which is accurate to within 1% for MeV particles:

$$\frac{dE}{dx} = -\frac{4\pi e^4 z^2}{m_e V^2} NZ[\ln \frac{2m_e V^2}{I} - \ln(1-\beta^2) - \beta^2] \qquad (17)$$

where z is the particle charge, Z is the charge of the stopping ions and V is the speed of incident ions.

The stopping power of deuterons and tritons up to their maximum knock-on energy, and protons up to their maximum energy produced by secondary reaction, is shown in Fig. 9. It is clear that if these are the only particles that are incident on the detector then if an unknown particle deposits an arbitrary $\delta E$, it could either be a triton, a lower energy deuteron or an even lower energy proton. Now, due to the knock-on cut-off energies, there are certain $\delta E$'s that provide immediate particle discrimination. For example, nothing but a 17.4 MeV proton can deposit 5 keV/$\mu m$ since deuterons and tritons with the necessarily high energies to deposit this little energy do not exist. In fact, all protons produced by the secondary reactions can be uniquely discriminated from deuterons and tritons in this way

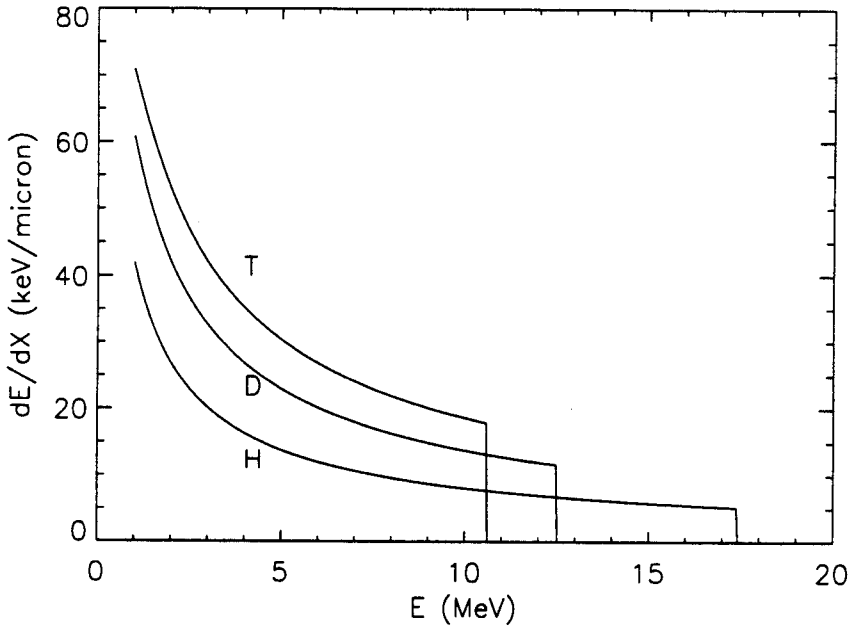


Figure 9: Stopping power (LET) in silicon of knock-on D and T ions and secondary protons as calculated from the Bethe-Bloch formula. These particles have maximum energies of 12.5 MeV, 10.6 MeV and 17.4 MeV. A semiconductor array, which has a sensitive depth thickness of about 20 $\mu$m, measures the energy deposition (and hence the LET) of a particle given by $\delta$E = (dE/dx)$\Delta$x where $\Delta x$ is the thickness of the sensitive depth. It can be seen that LET's below 12 keV/$\mu$m can only be due to the high energy protons ( $>$ 6 MeV) while a higher LET can be due to D or even T ions as well.

(of course < 14.1 MeV knock-on protons will produce the same signal). If 12 keV/$\mu m$ is recorded, the particle could either have been a 6 MeV proton or a 12.5 MeV deuteron. Thus at LET's above this, the signals may be due to either deuterons or protons. Similarly, at a higher LET, tritons will get mixed into the signal. Clearly, the sensitivity and energy resolution of the detector to $\delta E$ will need to be determined in order establish the energy resolution. This will need to be measured empirically.

Thus just a single layer semiconductor array which samples the LET of a particle is sufficient to provide some energy and particle discrimination. This is because the LET of a particle is a function of the energy to mass ratio and the fusion products have characteristic maximum energies. The remaining ambiguity is whether the signal is due to low energy protons, medium energy deuterons or high energy tritons.

## 7.2 A magnetic spectrometer coupled to the single layer photodiode system - full energy and mass resolution

The ambiguity may be removed by using a magnetic spectrometer. By placing a magnetic field at the detector aperture, the charged particles will be dispersed according to their energy and mass product. Hence if a few arrays are placed alongside each other in the path of the dispersed beam, each array will only be exposed to a particular energy$\times$mass window. It is found that with suitable positioning of the detectors and the use of a sufficient magnetic field, this extra particle and mass discrimination is enough that a particular $\delta E$ recorded in a particular detector can only have been produced by a particle with a particular mass and energy; unique particle discrimination has been achieved. This is depicted in Fig. 10 which is simply the stopping power plotted against the magnetic dispersion parameter, mass $\times$ energy. Fig. 11 shows particle trajectories for 7 MeV deuterons and 10.6 MeV tritons which have the same initial stopping power. The arrays must then be positioned far enough back that these two beams are not incident on the same array.

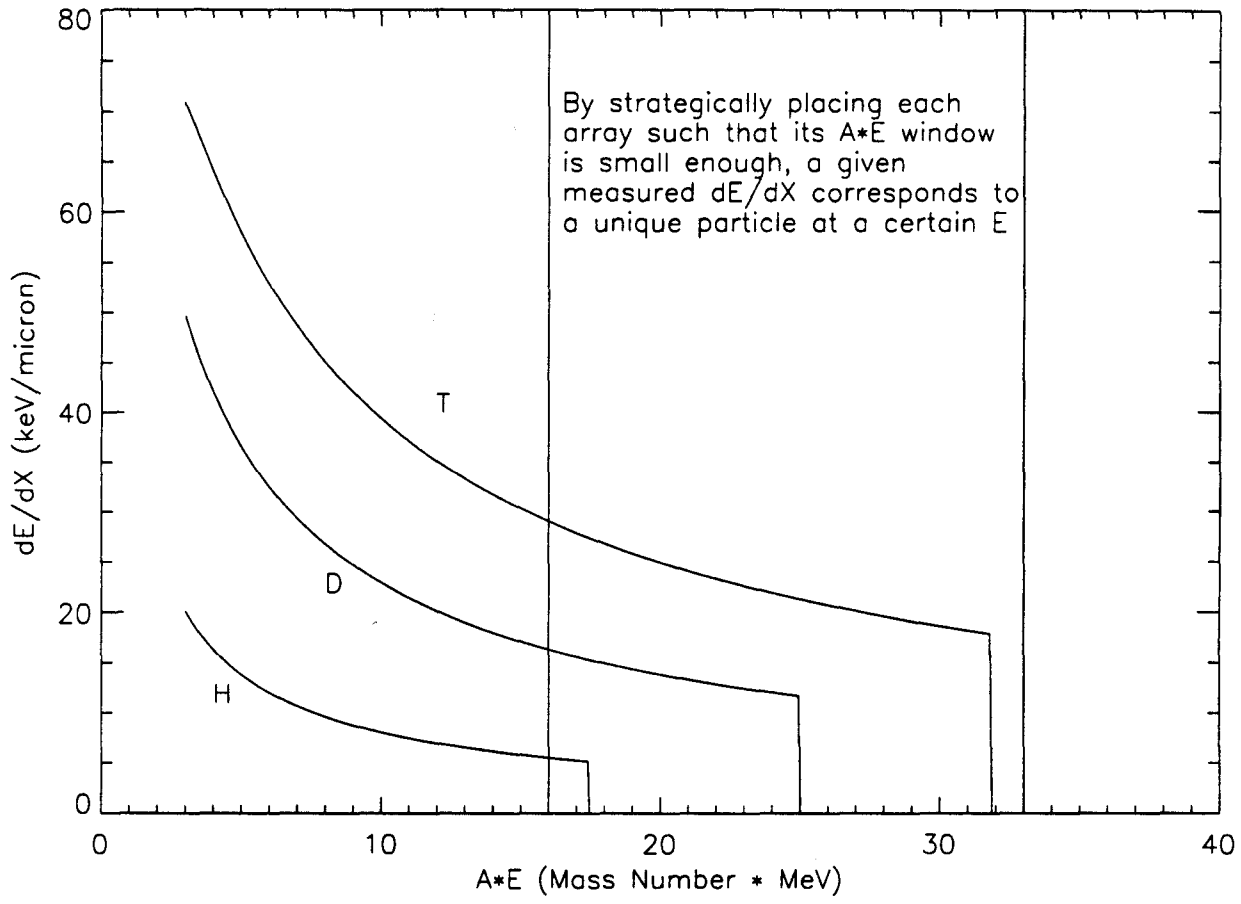


Figure 10: Stopping power (LET) in silicon of knock-on D and T ions and secondary protons as plotted against the magnetic dispersion parameter, mass×energy. The position of the detector in the dispersed ion beam defines a particular mass×energy window, viewed by the detector. Thus, within the A×E window, such as the one between the two vertical lines, there is a one-to-one correspondence between a measured $(dE/dx)\Delta x$ and the energy for a particle.

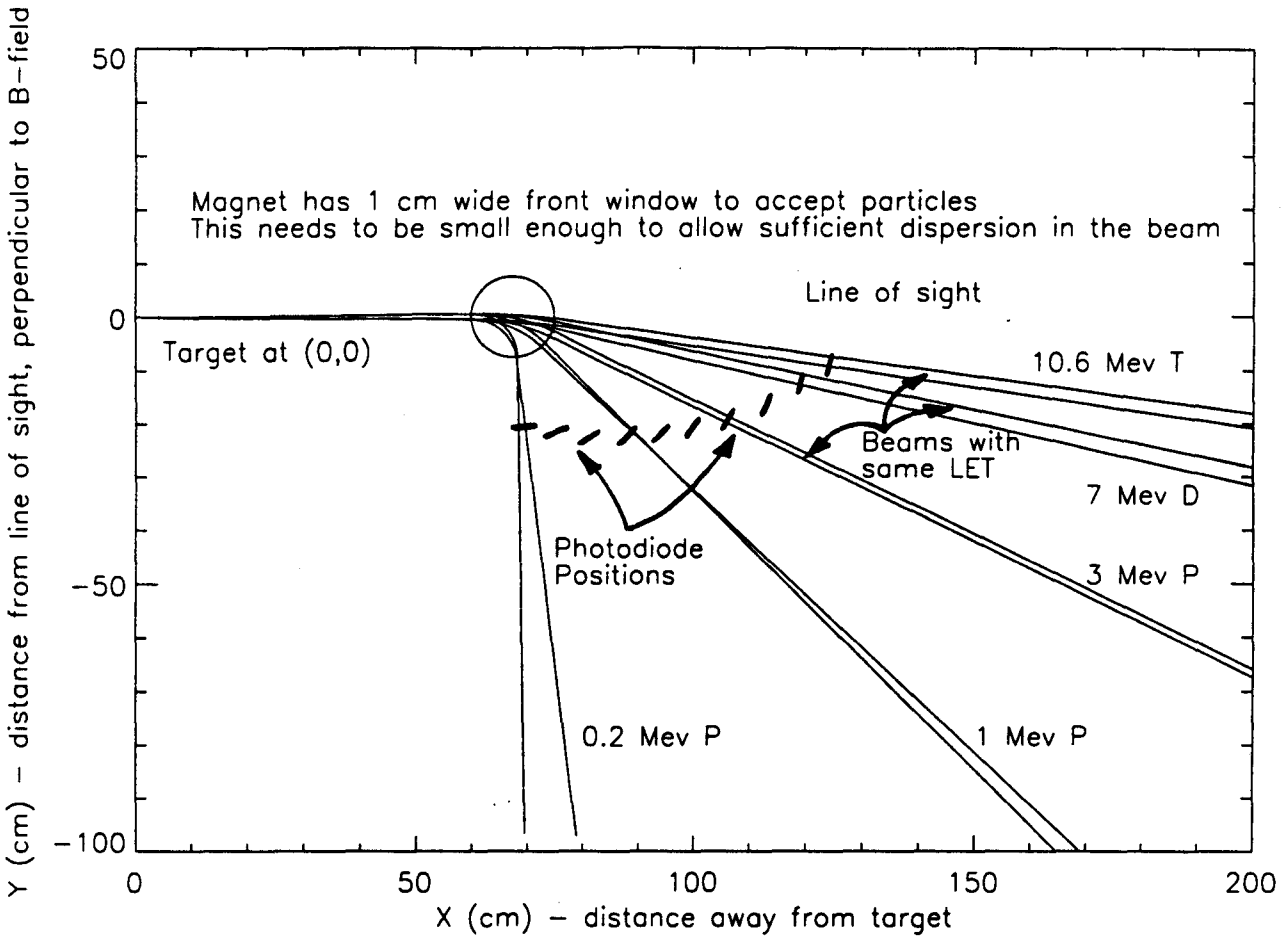


Figure 11: Ion trajectories through a 0.8 tesla dipole magnet placed 60 cm from the target with a 1 cm wide acceptance aperture. The detectors are strategically placed such that beams of different particles with the same linear energy transfer (LET) in silicon (such as 10.6 MeV tritons, 7 MeV deuterons and 3 MeV protons - see Fig. 9) are not incident on the same detector. With approximately 10 strategically placed photodiodes ($2500 apiece), the detector energy range is from 0.2 MeV up to > 17.4 MeV for protons.

## 7.3 Inverse operation

The above description of the system involves first measuring the LET of the particle and then using the magnet to resolve the particle identity ambiguity. In this mode of operation, essentially all of the energy resolution is being performed by the photodiode.

With the spatial dispersion of the particles due to the magnet and the extremely high spatial sensitivity of the photodiodes (typically 20 - 50 $\mu m$), information can also be obtained from the position of events on the photodiode. By first looking at the position of the event on the photodiode, one can obtain the mass×energy of the particle. This ambiguity may be resolved by examining the LET of the particle. Clearly, the energy uncertainty will be determined by the uncertainty in measuring mass×energy and not the uncertainty in the LET measurement (which involves difficulties with the sensitive depth). With a wide aperture this mass-energy product uncertainty may be high; however, if the signal is high enough that a small aperture may be used, and the photodiodes are positioned far enough away, the dispersion of the beam may be enough that uncertainties in mass×energy are less than those in LET.

Exactly which of the two modes of operation will be more suitable in different conditions will need to be examined in further detail.

# 8 Capabilities of this detector

## 8.1 Energy range

As can be seen from Fig. 11, by using a number of appropriately positioned arrays, the range of energies from 10.6 MeV tritons down to 0.2 MeV protons may be covered. It is thus likely that, even with significant slowing down of the 3 MeV proton in high $\rho R$ plasmas, the fusion yield can still be measured.

## 8.2 Energy resolution

While the energy resolution of the photodiodes needs to be resolved experimentally, the resolution of the magnetic spectrometer can be estimated from the trajectory plotter used to generate Fig. 11. For a 1 cm wide magnet aperture, the energy uncertainty for the 3 MeV protons is about 400 keV if the photodiodes are at 160 cm from the target, ie. due to the finite width of the aperture window, particles of 3±0.2 MeV may be incident on the same pixel element.

For the measurement of ion temperature, it is necessary to resolve 50 keV on either side of the 3 MeV proton line. A difference of 50 keV around 3 MeV corresponds to a difference of about 200 $\mu$m on a photodiode at 160 cm. If CCD's with 13.5 $\mu$m square pixels (EG&G RA 2000J) are used, this would spread the energy drop off of the DD reaction over about 15 pixels.

## 8.3 Output signal

Using $\rho R = 10\text{mg/cm}^2$, a 1:1 D to T ratio, $\sigma_d + \sigma_t = 1.5$ barns (the total elastic scattering cross section is used since the energy range of this detector extends down to 0.2 MeV), and a detector area of 2 $\text{cm}^2$ (2 cm high and 1 cm across the magnetic field) gives the knock-on signals shown in Fig. 12.

Now a 24" port has a cone angle given by arctan(28.0"/63.43") since the port flanges are 28.0" in diameter and the port is 63.43" from the target. If the face of the magnet directed towards the target has a maximum dimension of 10", then the magnet beam aperture could be brought as close as 60 cm to the target before violating the cone angle. (Heating limits would also need to be considered when more information becomes available.) At this distance and with $\rho R = 0.01$ g/$\text{cm}^2$, a neutron yield of $2\times10^9$ could provide 100 knock-on counts, while a $2\times10^{10}$ neutron yield would give 1000 counts.

It is possible to raise the count level by increasing the width of the magnet aperture allowing beam passage. However, with wider beams, the detectors would need to be placed further back behind and to the side of the detector in order to sufficiently disperse the beam to provide the necessary uniqueness in the $\delta E$ measurements. With a wider detector area, it would be impossible to fit the system into a TIM and thus the detector aperture would have to retreat to 160 cm, outside the vacuum chamber, lowering the count rate. A possible solution to this is to use a stronger magnet; however, it appears that the compact permanent magnets have a maximum field around 0.8 to 1 tesla. Clearly, high field electromagnets would not fit into the TIM.

The best way to increase the count level is to make the detector compact enough that it fits into a TIM since the solid angle is more strongly dependent upon the radial distance from the target ($\frac{1}{r^2}$) than on the size of the target window.

Fig. 13a gives the velocity averaged fusion cross section for DD and DT, which can be seen to be about 100 times less for DD than DT at a few keV. Now since the number of knock-ons is approximately 100 times less than the number of primary DT reactions, it follows that the total number of knock-ons and the total DD proton yield will be of the same order of magnitude. The D-$^3He$ reaction cross section is given in Fig. 13b and found to be 0.78 barns at 0.82 MeV, of similar order as the knock-on cross sections. Thus the count rate of secondary protons is likely to be two orders of magnitude less than that for knock-ons.

If, on the other hand, very high yields should be obtained, the great advantage of this detector is that the width of the magnet aperture may be reduced to prevent saturation of the detectors.

# 9 Component specifics and further design issues

## 9.1 Component specifics

In order to provide sufficient dispersion in a short distance, a magnetic field on the order of one tesla is required. The design depicted in Fig. 11 utilizes a 0.8 tesla, 15 cm diameter permanent dipole magnet, with 3 cm between pole faces. Magnetic Component Engineering has offered to build this system for $30,000. The magnet would weigh 225 lbs and have the

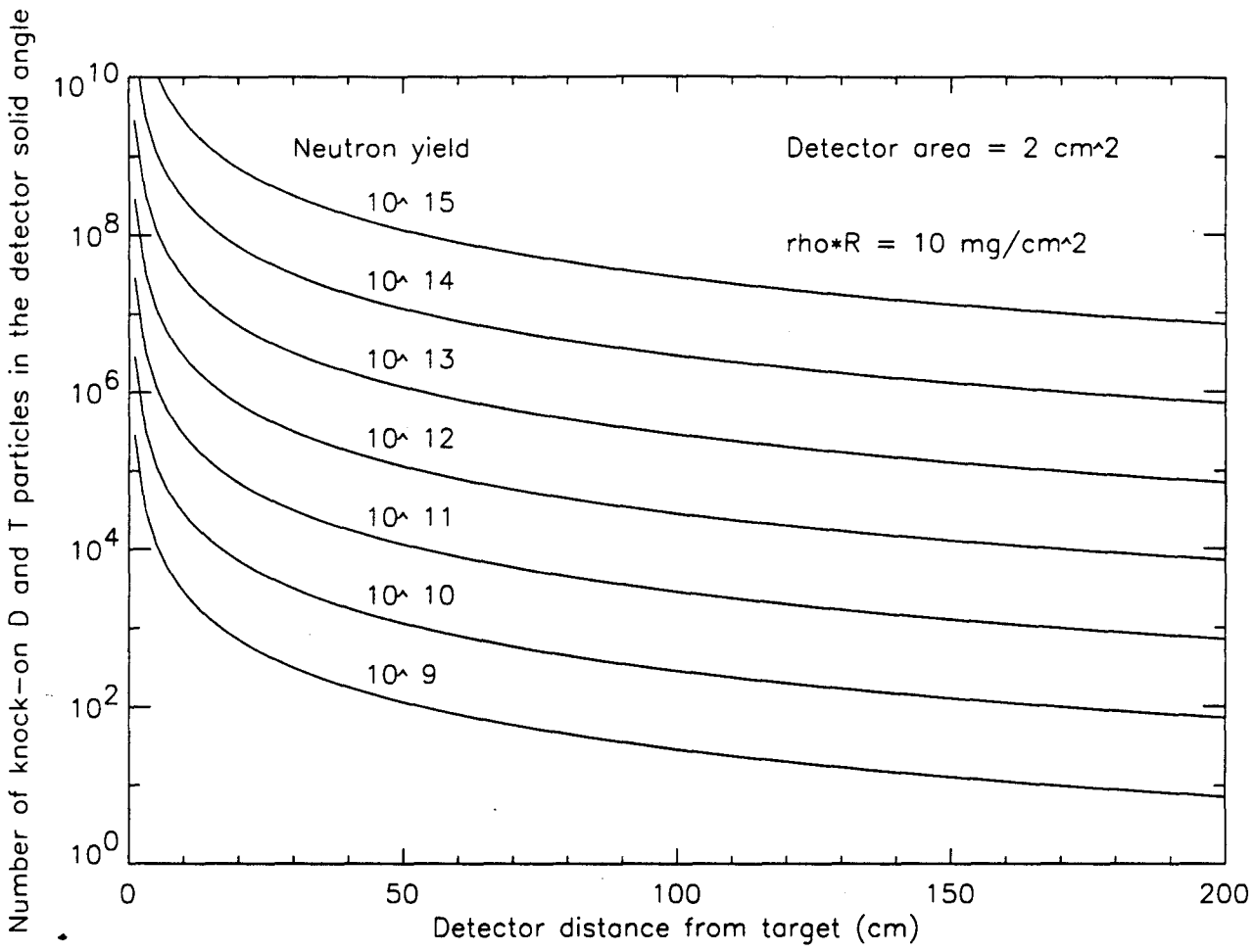


Figure 12: Number of D and T knock-ons captured in the solid angle defined by the magnet window of 2 $cm^2$. The magnet window may be as close as 60 cm to the target if the maximum front dimension of the magnet is 10" and the detector is located in a 24" port. The outside wall of the vacuum chamber is at about 160 cm. By varying the radial position of the detector window and using a variable aperture size, a large dynamic range may be accessed without saturating the detector.

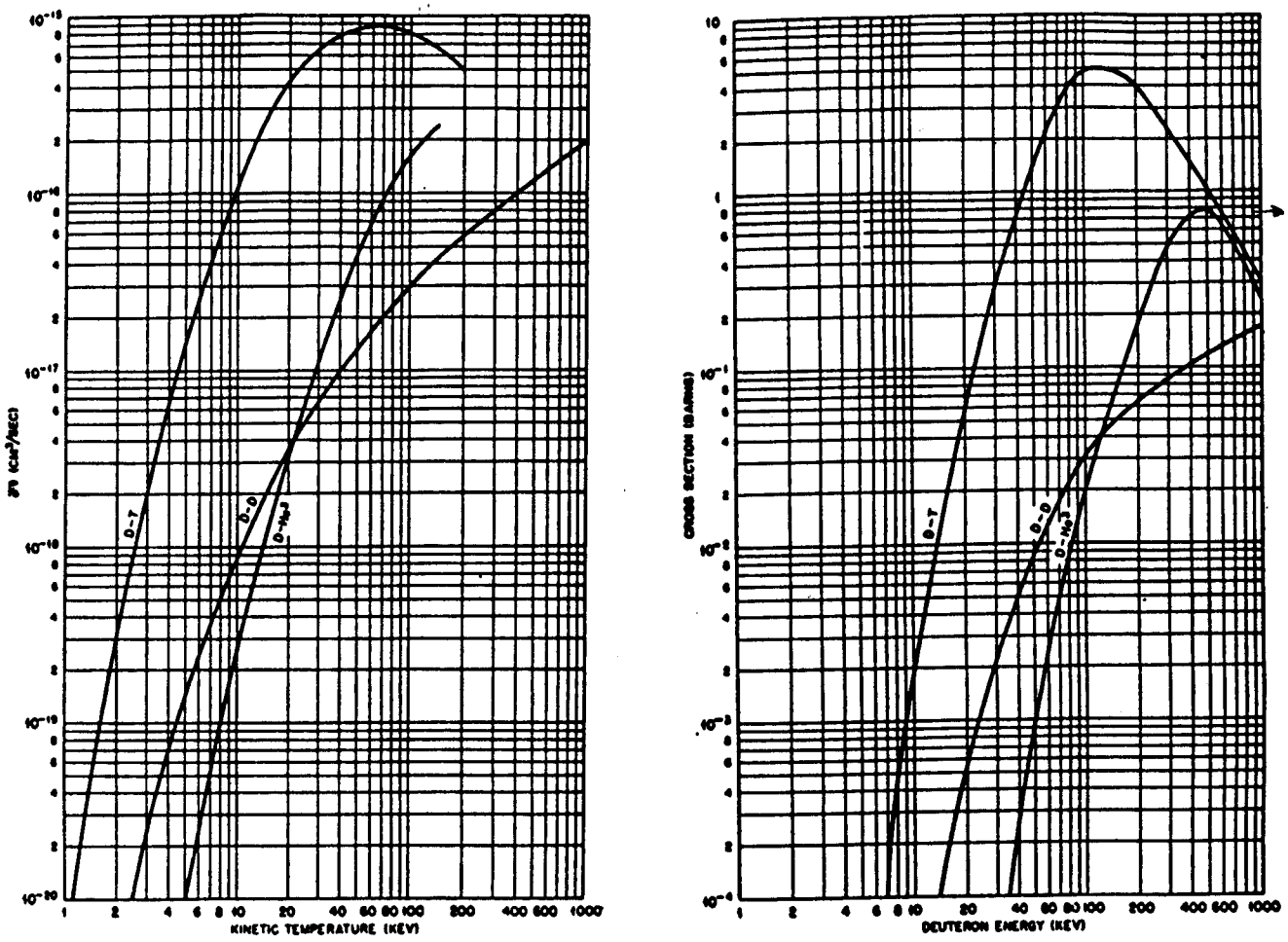


a) b)

Figure 13: a) Values of $\langle \sigma v \rangle$ based on a Maxwellian distribution for DT, DD and $D^3He$ reactions. In the realm of a few keV, the DT reaction rate is 100 times higher than the DD rate. Since approximately one in every hundred DT neutrons generates a knock-on, the yield of knock-ons and DD protons is of the same order. b) Cross-sections for DT, DD and $D^3He$ reactions. A $^3He$ energy of 820 keV corresponds to a D energy of 550 keV. At this energy, the fusion cross section is 0.78 barns. Thus the number of secondary D-$^3He$ protons is about 100 times less than the number of DD protons and DT neutron knock-ons.

largest dimension be 12". This appears to be a conservative estimate and it is reasonable that with further design and investigation, the maximum dimension could be reduced to less than 10" in order that the whole system fit into a TIM.

The most important criteria for the detector arrays in this design are a large detection area (or at least a minimum non-sensitive region between adjacent arrays) to cover the dispersed beam, and a sufficient number of pixels. The EG&G Reticon RA0640A array has 640×480 pixels per array, and 50 $\mu m$ square elements. Approximately four or more arrays would be required to cover the dispersed beam width. Each array costs $2490 (excluding the necessary driver electronics). Dimensions for this array are given in Fig. 14.

## 9.2 Further design issues

i Since the laser light is in the visible range and is easily reflected, this will be a large source of background for the light-sensitive photodiodes. Thus it will be necessary to have some protective cover over the magnet window, such as 1500 Å of Al. Such a layer will reduce the visible light intensity by many orders of magnitude with hardly any attenuation of the charged particles.

ii To increase the flexibility and dynamic range, the whole device should be retractable and have an adjustable aperture.

iii It may be possible to construct a taper for the front face of the magnet to allow deeper access into the port cone angle for increased signal.

iv The magnet should have minimum fringing fields; thus, the design must have suitable return paths for the fields.

# 10 The Cockcroft-Walton testing facility

Throughout this report, references have been made to the usefulness of the Cockcroft-Walton facility in verifying critical steps in the diagnostic development. Specifically, we can generate proton energies from 0.2 – 16 MeV as well as a spectrum of energies for deuterons, tritons and $\alpha$'s. It is important to note that much of the spectrometer testing will have to be done in vacuum. Our facility has the capability to do this. It is also absolutely calibrated.

# 11 Issues to investigate in the next phases

The following is a list of important issues which need to be addressed in the next stages of the program:

1 **Sensitive depth**: The effective sensitive depth of the photodiode to charged particles needs to be determined. An experimental program using 0.2 – 16 MeV charged particles from our Cockcroft-Walton facility will be carried out to address this issue. (Although more expensive, thinned, back-illuminated CCD's from Lincoln Labs (MIT) would eliminate this concern.)

Conditions: 25°C, Data Rate 2 MHz, Integration time 170 ms. Voltage levels set to typical values shown in Table 1

| Parameter | Sym | Min | Typ | Max | Units |
|---|---|---|---|---|---|
| Format | | | 640 x 480 | | |
| Pixel size | | | 50 x 50 | | µm |
| Imaging area | | | 32 x 24 | | mm |
| Dynamic range | DR | | 1500:1 | | rms |
| Saturation voltage | $V_{sat}$ | | 300 | 500 | mV |
| Dark current | DL | | 0.1 | | $nA/cm^2$ |
| Saturation exposure [1] | Esat | | .1 | | $\mu J/cm^2$ |
| Responsivity | R | | 3 | | $V/\mu J/cm^2$ |
| Photo response nonuniformity | PRNU | | 10 | 15 | ±% |
| Noise equivalent exposure | NEE | | .07 | | $nJ/cm^2$ |
| DC power dissipation | $D_{dc}$ | | 50 | | mW |
| Operating frequency | $f_{clock}$ | | 1 | 5 | MHz |
| Read out noise | | | 200 | | µV (rms) |

Note:
[1] Light source is 2870°K tungsten lamp with a HA-11 visible spectrum filter.

**Table 4. Absolute Maximum Ratings**

Voltages: measured WRT substrate

| | Min | Max |
|---|---|---|
| Storage temperature | -55°C | +85°C |
| Operating temperature | -55°K | 50°C |
| Voltages: measured WRT substrate | 0V | 15V |

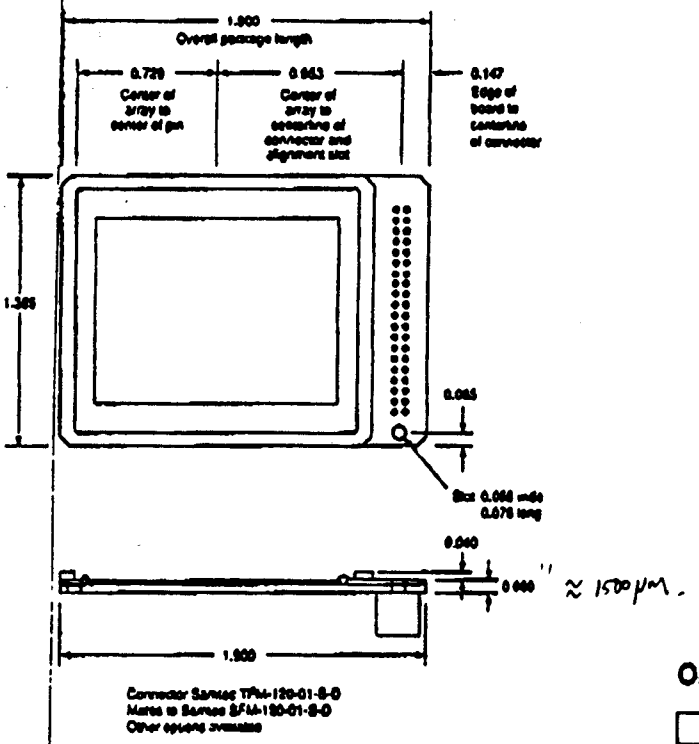


Figure 5. Package Dimensions

**Ordering Information**

| Part Number |
|---|
| RA0640ANN-011 |

055-0373
June 1994



Figure 14: Dimensions and specifications for the RA0640A silicon photodiode array manufactured by EG&G Reticon.

2 **Transient neutron response**: The transient response of the photodiodes to 2.5 MeV and 14.1 MeV neutrons must be determined. We have reason to believe that, due to the thin sensitive layer in the photodiode, neutrons will not significantly interfere with the charged particle signal. We will use 2.5 MeV and 14.1 MeV neutrons from our Cockcroft-Walton accelerator to verify this.

3 **Cooling requirements**: We will test the signal response of the photodiodes to 0.2 – 16 MeV charged particles in uncooled and, if necessary, cooled configurations.

4 **Blooming and saturation**: Tests need to be performed to establish whether these factors significantly affect the signal response. Once again, the more expensive, thinned, back-biased CCD's from MIT Lincoln Labs would eliminate the blooming concern.

5 **Energy resolution**: We need to determine the energy resolution of the entire system – magnet, photodiode, and magnet aperture – using 0.2 - 16 MeV charged particles generated by our Cockcroft-Walton accelerator.

6 **Surrounding electronics**: The surrounding electronic configuration and support structure for the photodiodes needs to be carefully examined and tested for issues such as crosstalk and pickup.

7 **Magnet design**: It is critical that the magnet be compact to enable the spectrometer to get as close as possible to the target. Also, the magnet must have minimum fringing fields.

8 **Pusher effects**: The effect of pusher $\rho\Delta R$ on charged particle slowing down needs to be investigated. For example, if $\rho\Delta R \sim 0.2$ g/cm$^2$, the charged particle signal will be severely attenuated. Also, the proton background from CH pushers needs to be more carefully addressed.

9 **Charged particle slowing down in plasmas**: Since the proposed spectrometer can measure particle energies down to 0.2 MeV, calculations need to be made to determine the slowing down of knock-ons and secondary protons in a plasma at these low energies (see e.g. the calculations by C.K.Li in Fig. 6). Furthermore, the possibility of determining the spatial burn profile from the charged particle spectra needs to be studied.

10 **$^3$He doping**: We will investigate doping with $^3$He in both DD and DT so as to generate 14.7 MeV protons. This could provide a good measurement of temperature and slowing down as well as a measurement of yield at a high $\rho R$ (and high temperature).

11 **Radiation damage**: Limited tests will be carried out on the Cockcroft-Walton to ensure that radiation damage will not be a problem with neutron fluences typical of OMEGA Upgrade.

12 **Costs**: Full program costs such as magnet, photodiodes, spectrometer components (variable aperture, vacuum pump, vacuum components, ...), assembly, critical tests, etc. need to be carefully estimated.

# Conclusion

The preliminary design for a charged particle spectrometer using 10 or more photodiodes and a permanent magnet has been investigated. With this design, D, T and H knock-ons and secondary protons may be measured from 0.2 MeV up to 18 MeV, and 100 knock-ons can be detected with a yield as low as $10^9$ DT neutrons when the spectrometer aperture is 60 cm from the implosion. With about $10^6$ picture elements over an individual photodiode, with virtually each element being a single-hit detector, the dynamic range for this spectrometer is from $1 - 10^5$ charged particles. The variable aperture window extends this dynamic range even further.

The theory for $\rho R$ measurements using the knock-on and secondary reaction method has been reviewed in the light of our proposed system which can highly resolve energy spectra as well as uniquely identify different particles (ie. H, D, T, $^3$He and $^4$He). With a charged particle spectrum, not only is the $\rho R$ limit raised up to 0.3 g/cm$^2$ (if hydrogen doping is used), the fusion yield and $T_i$ can also be measured. Significantly, by placing two of these portable spectrometers at very different positions around the OMEGA Chamber, the resulting charged particle spectra and yield measurements will allow the measurement of implosion and burn symmetry.

# Acknowledgements

This work was supported in part by the Laboratory for Laser Energetics (University of Rochester); in part by the Department of Energy; and in part by Lawrence Livermore National Laboratory.

# References

[1] S. Skupsky, and S. Kacenjar, J. Appl. Phys.**52**, 2608 (1981).

[2] S. Kacenjar, S. Skupsky, A. Entenberg, L. Goldman, M. Richardson, Phys. Rev. Lett.**49**, 463 (1982).

[3] S. Kacenjar, L. M. Goldman, A. Entenberg, and S. Skupsky, J. Appl. Phys.**56**, 2027 (1984).

[4] J. Nakaishi, N. Miyanaga, H. Azechi, M. Yamanaka, T. Yamanaka, M. Takagi, T. Jitsuno, and S. Nakai, Appl. Phys. Lett.**54**, 1308 (1989).

[5] T. E. Blue, J. W. Blue, J. S. Durham, D. B. Harris, A. S. Hnesh, and J. J. Reyes, J. Appl. Phys. **54**, 615 (1983).

[6] H. Azechi, N. Miyanaga, R. O. Stapf, K. Itoga, H. Nakaishi, M. Yamanaka, H. Shiraga, R. Tsuji, S. Ido, K. Nishihara, Y. Izawa, T. Yamanaka, and C. Yamanaka, Appl. Phys. Lett.**49**, 555 (1986).

[7] H. Azechi, M. D. Cable, and R. O. Stapf, Laser and Particle Beams **9**, 119 (1991).

[8] E. M. Campbell, S. M. Lane, Y. L. Pan, J. T. Larsen, R. J. Wahl, and R. H. Price, J. Appl. Phys.**51**, 6062 (1980).

[9] National Neutron Cross Section Center, BNL 400, Third Edition, (1970)

[10] I. Hutchinson, Principles of Plasma Diagnostics, (Cambridge University Press, 1992), pg. 315.

[11] EG&G Image Sensing Products, 1992/1993 Catalog.

[12] T. S. Lomheim, R. M. Shima, J. R. Angione, W. F. Woodward, D. J. Asman, R. A. Keller, and L. W. Schumann, IEEE Trans. Nucl. Sci.**37**, 1876 (1990).

[13] J. U. Schott, Nucl. Tracks Radiat. Meas. **15**, 81 (1989).

[14] E. H. M. Heijne, and P. Jarron, Nucl. Inst. Methods **A275**, 467 (1989)